J. Am. Soc. Mass Spectrom. (2017) 28:1282–1292
DOI: 10.1007/s13361-017-1669-0

FOCUS: BIO-ION CHEMISTRY: INTERACTIONS OF BIOLOGICAL IONS WITH IONS, MOLECULES, SURFACES, ELECTRONS, AND LIGHT : RESEARCH ARTICLE

Collisional Cross-Sections with T-Wave Ion Mobility Spectrometry without Experimental Calibration

Daniel N. Mortensen, Anna C. Susa, Evan R. Williams

Department of Chemistry, University of California, Berkeley, CA 94720-1460, USA

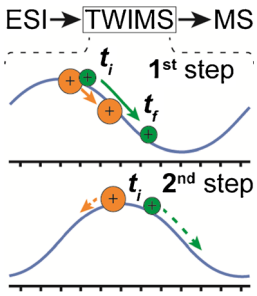

Abstract. A method for relating traveling-wave ion mobility spectrometry (TWIMS) drift times with collisional cross-sections using computational simulations is presented. This method is developed using SIMION modeling of the TWIMS potential wave and equations that describe the velocity of ions in gases induced by electric fields. The accuracy of this method is assessed by comparing the collisional cross-sections of 70 different reference ions obtained using this method with those obtained from static drift tube ion mobility measurements. The cross-sections obtained here with low wave velocities are very similar to those obtained using static drift (average difference = 0.3%) for ions formed from both denaturing and buffered aqueous solutions. In contrast, the cross-sections obtained with high wave velocities are significantly greater, especially for ions formed from buffered aqueous solutions. These higher cross-sections at high wave velocities may result from high-order factors not accounted for in the model presented here or from the protein ions unfolding during TWIMS. Results from this study demonstrate that collisional cross-sections can be obtained from single TWIMS drift time measurements, but that low wave velocities and gentle instrument conditions should be used in order to minimize any uncertainties resulting from high-order effects not accounted for in the present model and from any protein unfolding that might occur. Thus, the method presented here eliminates the need to calibrate TWIMS drift times with collisional cross-sections measured using other ion mobility devices.

Keywords: Traveling wave, Ion mobility, Mass spectrometry, Collisional cross-sections

Received: 26 August 2016/Revised: 21 March 2017/Accepted: 27 March 2017/Published Online: 21 April 2017

Introduction

Ion mobility spectrometry (IMS) separates gaseous ions on the basis of their collisional cross-sections, which depend on ion shape, mass, charge state, temperature, and ion-neutral interactions [1]. IMS has been used in many applications, including the separation of atomic ions [2, 3], small clusters [3–5], tryptic digests [6–9], and investigating the gas-phase conformations of biopolymers [10–13], biopolymer complexes [14–16], and viruses [17]. IMS can be done using static drift tube [18–20], field-asymmetric [20–23], aspiration [24, 25], and traveling-wave [26, 27] IMS devices. In traveling-wave IMS (TWIMS), a potential wave is generated by applying a DC potential to a set of adjacent ring electrodes, and this wave is moved through the device with time [28]. Some ions traverse the device at the velocity of the wave, and others are overtaken by the wave, resulting in ion separation [28, 29]. The shape of the wave and the distance between consecutive waves can differ between TWIMS devices depending on instrument design and parameters [27].

In static drift tube (DT)IMS, ion cross-section can be directly determined from the measured ion drift times when all experimental parameters are accurately known or by calibrating with ions with known collisional cross-sections [30–32]. Determining ion cross-sections with TWIMS is typically done by calibrating the drift times to collisional cross-sections measured using DTIMS [33–36]. Cross-sections obtained for ions generated from denaturing solutions using TWIMS chemical calibration techniques are generally very similar to those obtained using DTIMS (average difference = 1%) [34, 37–39], although differences in cross-sections as high as 9% have been reported [39]. Obtaining accurate collisional cross-sections for ions generated from buffered aqueous solutions in which the proteins have native conformations and activities using

Electronic supplementary material The online version of this article (doi:10.1007/s13361-017-1669-0) contains supplementary material, which is available to authorized users.

Correspondence to: Evan R. Williams; *e-mail:* erw@berkeley.edu

TWIMS is often more challenging [38, 40]. This is because the drift times of protein ions formed from buffered aqueous solutions in which proteins are folded increase more rapidly with increasing wave velocity than do the drift times of ions formed from solutions in which proteins are denatured. This difference in behavior has been attributed to collisional heating and subsequent unfolding of initially folded protein ions during TWIMS [41] and also to unspecified characteristics of the TWIMS separation mechanism [38]. Methods for obtaining collisional cross-sections of ions formed from buffered aqueous solutions have been presented and rely on selecting calibrant ions that have similar rates of change in drift time with TWIMS wave velocity as the ions of interest [38, 40].

A method for directly measuring the mobility of ions using TWIMS was reported [42]. SIMION modeling was used to derive an equation that relates the ion mobility and the wave velocity to the minimum wave height required to cause an ion to traverse the TWIMS device at the velocity of the wave. The minimum wave height is determined by incrementally increasing the wave height until the ion traverses the device at the wave velocity. Cross-sections obtained using this method are the same within 5% as those obtained with DTIMS [42]. However, even though the motion of ions in TWIMS devices has been modeled [43, 44], there are currently no methods that enable cross-sections to be determined from a single TWIMS drift time measurement without prior calibration [14, 29, 36, 45].

Here, a method for relating TWIMS drift times with collisional cross-sections using computational simulations is presented. This method is developed using SIMION modeling of the TWIMS potential wave and equations that describe the velocity of ions in gases under the influence of electric fields. Cross-sections obtained using this method under conditions of low wave velocities are very similar to those obtained with DTIMS (average difference = 0.3%) for ions formed from both denaturing and buffered aqueous solutions. At high wave velocities, the collisional cross-sections obtained using the computational method presented here are significantly larger (as much as 32% larger) than those obtained with DTIMS, especially for ions formed from buffered aqueous solutions. These higher cross-sections may result from high-order effects not accounted for in the simple model presented here, although some protein unfolding during TWIMS as a result of collisional ion heating [41, 46–48] may also contribute. Results from this study show that ion collisional cross-sections can be determined from single TWIMS drift time measurements but that low wave velocities and gentle instrument settings should be used to reduce any uncertainties resulting from high-order effects not accounted for in this model and from any protein unfolding that might occur during the measurement.

Experimental

Experiments are performed using a Synapt G2 high definition mass spectrometer (Waters Corp., Milford, MA, USA). Ions are formed by nanoESI using borosilicate capillaries with tips pulled using a model P-87 Flaming/Brown micropipette puller (Sutter Instruments Co., Novato, CA, USA). A platinum wire is brought into contact with the sample solution inside the capillary, and nanoESI is initiated by applying a ~800 V potential to the platinum wire relative to the potential of the entrance of the mass spectrometer. Flow rates in the helium and TWIMS cells are kept constant at 180 and 90 mL/min, respectively. The pressure in the TWIMS cell is measured using a model APG-L active Pirani gauge (Edwards, Crawley, UK) that is located within the TWIMS chamber, and this value was 3.2 mbar in all experiments. The measured drift times are adjusted by subtracting the time required for the ions to traverse the transfer TWIMS cell, which is located immediately after the TWIMS cell and immediately prior to the mass analyzer. This time is ~142 μs and is determined by dividing the 10 cm length of the transfer cell by the 703 m/s wave velocity used in the transfer cell, as described previously [33]. With some wave conditions, low mobility ions do not traverse the TWIMS cell within the time frame of a single drift experiment. When this occurs, the measured drift times are adjusted by adding the 36.268 ms length of a single drift experiment. Two hundred drift bins are used for all experiments, resulting in a bin width of ~181 μs. SIMION ver. 8.0 [49] is used to model the electric field along the axis of the TWIMS device using a pixel size of 0.10 mm. This pixel size was selected by incrementally decreasing the pixel size until the electric field strength no longer significantly changed with pixel size. The electric field strength changes by less than 1% at all points along the axis of the device as the pixel size decreases from 0.20 to 0.05 mm.

Bovine serum albumin, ubiquitin, equine cytochrome *c*, myoglobin, concanavalin A from *Canavalia ensiformis*, bradykinin, angiotensin II, and DL-polyalanine were obtained from Sigma-Aldrich (St. Louis, MO, USA), and acetonitrile, glacial acetic acid, and methanol were from Fisher Scientific (Fair Lawn, NJ, USA). Solutions were prepared in 18.2 MΩ water from a Milli-Q water purification system (Millipore, Billerica, MA, USA). Polyalanine solutions were prepared with 0.1 mg/mL analyte concentrations, and all other solutions were prepared with 10 μM analyte concentrations. Serum albumin and concanavalin A ions are formed from 200 mM aqueous ammonium acetate solutions in which they have native-like conformations and activities. Denatured polyalanine ions are formed from a 49/49/2 water, acetonitrile, acetic acid solution, and all other denatured protein and peptide ions are formed from 49/49/2 water, methanol, acetic acid solutions. DTIMS cross-sections for polyalanine were from reference [40], and all other DTIMS cross-sections were from reference [39]. All DTIMS cross-sections were measured in nitrogen gas [39, 40].

Calculations

Modelling the TWIMS Electric Potential

The ion drift velocity, v, is the average velocity of an ion in a gas that is induced by an electric field [31, 32] and is defined in Equation 1:

$$v = KE \quad (1)$$

where E is the electric field strength and K is the ion mobility. This equation is valid when the force applied to an ion by the electric field is equal but opposite to that resulting from momentum transfer resulting from collisions between the ion and the background gas. Energy imparted by the electric field is balanced by the loss of kinetic energy resulting from collisions with the background gas. For convenience, the condition wherein the magnitudes of these two forces are equal but opposite is defined here as force-balance. The mobility of an ion is described by the Mason-Schamp Equation [1]:

$$K = \frac{3ze}{16N}\left(\frac{2\pi}{\mu k_b T}\right)^{1/2}\frac{1}{\Omega} \quad (2)$$

where z is the ion charge state, e is the elementary charge, N is the background gas number density, μ is the reduced mass between the ion and the background gas, k_b is Boltzmann's constant, T is the background gas temperature, and Ω is the ion cross-section. The background gas number density describes the pressure in the drift cell. The background gas identity affects the reduced mass in Equation 2, although a term taking into account the interaction potential with the background gas is not included. Equations 1 and 2 are only valid under the 'low-field limit,' where the ratio between electric field strength and background gas pressure is low. The low-field limit varies with ion identity, but typical values range between ~15 and ~34 V cm^{-1} $mbar^{-1}$ [50, 51].

In order to determine the ion drift velocity using Equation 1, the electric field strength must be known. The geometry of the electric field varies between TWIMS devices depending on instrument design [27]. In a second generation TWIMS device, such as that used in these experiments, the electric field is generated by applying a DC potential with an amplitude referred to as the "wave height" to two consecutive plate pairs, followed by two plate pairs held at instrument ground, and this pattern is repeated throughout the device [27]. The electric field is varied incrementally with time by stepping the DC potential forward by a single plate pair. The electric potential and electric field strength along the axis of a second generation TWIMS device at a given point in time obtained with SIMION using a 40 V wave height are shown as blue lines in Figure 1a and b, respectively. The results in these simulations are obtained without an ion-gas collision model (i.e., these data are not from ion simulations but are simply the solutions to the Laplace equations along the axis of the TWIMS device at a discrete point in time). The effective wave height obtained with SIMION is equal to ~89.6% of the applied wave height potential (Figure 1a), consistent with the ~90% value reported previously [27]. The electric potential along the axis of the device (Figure 1a) appears to be mostly sinusoidal, whereas the electric field strength (Figure 1b) resulting from this electric potential appears to have both sinusoidal and triangular wave characteristics.

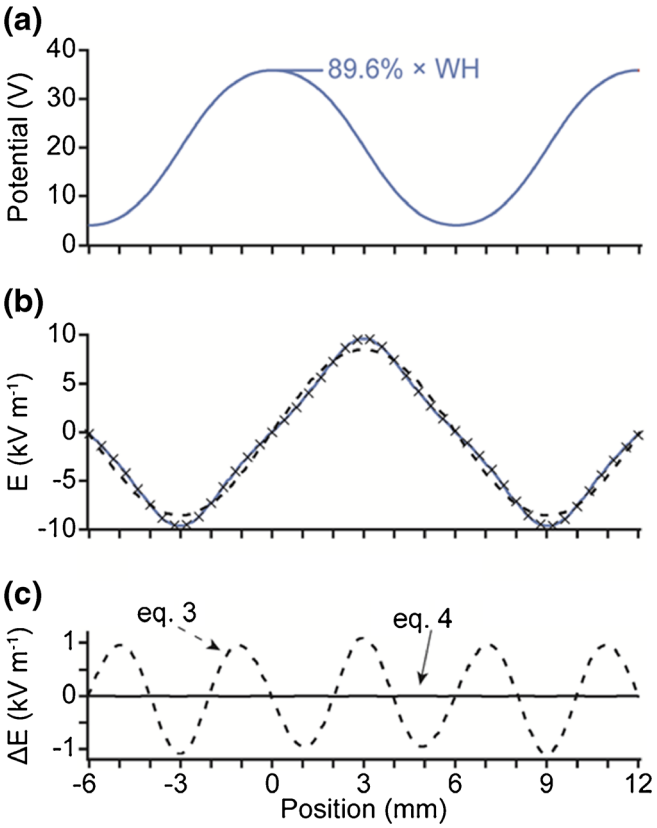

Figure 1. **(a)** The electric potential and **(b)** the electric field strength along the axis of a SYNAPT G2 high definition mass spectrometer TWIMS device obtained with a 40 V wave height using SIMION (blue lines), Equation 3 (black dashed line), and Equation 4 (black "x"s). **(c)** The difference between the electric field strength along the axis of the TWIMS device obtained with SIMION compared to that obtained with Equation 3 (dashed line) and Equation 4 (solid line). "WH" denotes wave height

The electric field strength obtained with SIMION (blue line, Figure 1b) is modeled as a sine wave (Equation 3):

$$E = A\sin(\theta x) \quad (3)$$

where A is the wave amplitude, θ is the wave frequency, and x is the ion position along the axis of the TWIMS device. For convenience, $x = 0$ is defined as the position at which the maximum electric potential occurs (see Figure 1a). The values of A and θ are listed in Table 1. The electric field strength obtained with Equation 3 for a 40 V wave height is shown as a black dashed line in Figure 1b. The difference between the electric field strength obtained with SIMION and that obtained from Equation 3 is shown as a black dashed line in Figure 1c. There are significant differences (≤11.4%) between the two electric field strengths (Figure 1c), indicating that the electric field strength is only crudely modeled by a single sine wave.

A linear combination of three sine waves can more accurately model the electric field strength (Equation 4):

$$E = A_1\sin(\theta x) + A_2\sin(3\theta x) + A_3\sin(5\theta x) \quad (4)$$

Table 1. Parameters for Equations 3 and 4. "WH" Denotes the Wave Height

θ	519.5 m^{-1}
A	WH × 213.5 m^{-1}
A_1	WH × 213.7 m^{-1}
A_2	WH × –25.1 m^{-1}
A_3	WH × 2.0 m^{-1}

where A_1, A_2, and A_3 are the amplitudes of the different waves, respectively (Table 1). The electric field strength along the axis of the TWIMS device obtained with Equation 4 for a 40 V wave height is shown as black "x"s in Figure 1b, and the difference between this electric field and that obtained with SIMION is shown as a solid black line in Figure 1c. The difference between these electric field strengths is less than 0.1% at all positions (Figure 1c), indicating that the electric field strength along the axis of the TWIMS device is modeled significantly more accurately by Equation 4 than by Equation 3.

Calculating Ion Drift Times

Because the electric field strength is not homogenous throughout the TWIMS device, the ion drift velocity changes with the ion position and, thus, with time as the ion travels through the device. Therefore, a time-dependent function is required to describe the motion of ions through the device. Velocity in a TWIMS device is given by the change in position over time:

$$\mathrm{v} = \frac{\mathrm{dx}}{\mathrm{dt}} \tag{5}$$

where t is time. In this model, we make the gross approximation that the average velocity in the TWIMS device is equal to the drift velocity defined in Equation 1, recognizing that the assumption of force balance required for Equation 1 is not met by this approximation. With this rough approximation, Equations 1 and 5 can be combined to obtain Equation 6:

$$\frac{\mathrm{dx}}{\mathrm{dt}} = KE \tag{6}$$

Different equations describing the motion of ions through the TWIMS device are derived by combining Equation 6 with Equations 3 and 4, respectively. Combining Equation 6 with Equation 3 and rearranging results in Equation 7:

$$KA\mathrm{dt} = \frac{\mathrm{dx}}{\sin(\theta \mathrm{x})} \tag{7}$$

This equation is integrated over a period of time equal to the duration of a single wave step. This duration of time is known as the "dwell" time (t_{dwell}) and is equal to the 254 mm length of the TWIMS device divided by the wave velocity. Integrating Equation 7 over the dwell time and rearranging results in Equation 8:

$$\mathrm{x}_t = \frac{2}{\theta}\tan^{-1}\left[\tan\left(\frac{\theta \mathrm{x}_o}{2}\right)\exp(KAt_{dwell})\right] \tag{8}$$

where x_o and x_t are the ion positions at t = 0 and t_{dwell}, respectively. This equation can be used to determine the distance an ion travels through the device during a single wave step ($x_t - x_o$) as a function of the initial ion position and dwell time.

Combining Equation 6 with Equation 4 and rearranging results in Equation 9:

$$K\mathrm{dt} = \frac{dx}{A_1\sin(\theta \mathrm{x}) + A_2\sin(3\theta \mathrm{x}) + A_3\sin(5\theta \mathrm{x})} \tag{9}$$

The right side of Equation 9 cannot readily be integrated explicitly over time. Therefore, Equation 9 is integrated numerically from t = 0 to t_{dwell} using MatLab. An implicit approximation in both Equations 8 and 9 is that force-balance is achieved instantaneously, and thus the velocity of an ion changes instantaneously with the change in electric field strength. Therefore, when an ion reaches a position where the electric field strength is zero (i.e., x = –6.05, 0, and +6.05 mm, Figure 1b), the ion stops moving. In a TWIMS device, the strength of the electric field experienced by an ion changes continuously with time. Force-balance requires a finite amount of time to be achieved after the electric field strength changes [52, 53]. Therefore, force-balance is never fully achieved during TWIMS separations. Another approximation in this model is that the ions remain strictly confined to the axis of the device by the confining RF. Off axis, the electric field strength increases in square-wave characteristics. Off-axis motion is not accounted for in Equations 8 or 9 but may result in peak broadening as ions on axis will drift at a different velocity than ions that are off axis.

The total distance an ion travels when multiple waves pass through the device is obtained by summing the distance the ion travels during each wave step. The initial ion position in the first computational wave step is arbitrarily set to 1 mm, but starting the ion at different positions on the wave results in the same transit time to within 1%. The final ion position in this wave step is computed from the initial ion position and the instrument dwell time. The potential wave is then stepped forward, resulting in a change in the electric field strength experienced by the ion. The distance the ion travels during this new wave step is then computed as a function of the initial ion position in this wave step and the instrument dwell time. The potential wave is stepped forward and the distance the ion travels during each step is computed over multiple wave steps until the motion of the ion through the device is well characterized.

In order to simulate the motion of an ion as it traverses the TWIMS cell under different conditions, wave parameters are selected that result in an ion traversing the cell at the wave velocity and in the same ion being overtaken by the traveling waves. In order to simulate an ion traversing the TWIMS cell at the wave velocity, a 100 m/s wave velocity and a 40 V wave height are used. For convenience, the ion cross-section times the square root of the reduced mass per unit charge ($\Omega\,\mu^{1/2}\,z^{-1}$) is defined here as the adjusted cross-section. Ion mobility

is inversely proportional to the adjusted cross-section (Equation 2). A representative plot of the total distance traveled by an ion with an adjusted cross-section of 17.0 nm^2 $Da^{1/2}$ as a function of the number of times the wave is stepped through the device is shown in Figure 2a. This adjusted cross-section corresponds to the 14+ charge state of bovine serum albumin, which traverses the TWIMS device at the wave velocity with the parameters used to obtain Figure 2a but is overtaken by the waves with higher wave velocities. The results in Figure 2a are obtained with Equation 8 (black dashed line) and numerical integration of Equation 9 (blue line). The results obtained with both Equations 8 and 9 indicate that the ion traverses the 254 mm length of the device after the wave is stepped forward 84 times, which is the same as the number of plate pairs in the device, indicating that the ion traversed the device at the wave velocity.

In order to simulate this same ion under conditions where it is overtaken by the traveling waves, a 2000 m/s wave velocity and a 20 V wave height are used (Figure 2b). The results in Figure 2b are obtained with Equation 8 (black dashed line) and Equation 9 (blue line). When the ion is on the front of the wave, it moves forward through the device towards the mass analyzer, but when it is overtaken by a wave, it moves backwards through the device away from the mass analyzer (Figure 2b). Thus, the position of the ion inside the TWIMS device oscillates as waves are stepped through the device. The results in Figure 2b obtained with both Equations 8 and 9 indicate that under the conditions used here, the ion is overtaken by the

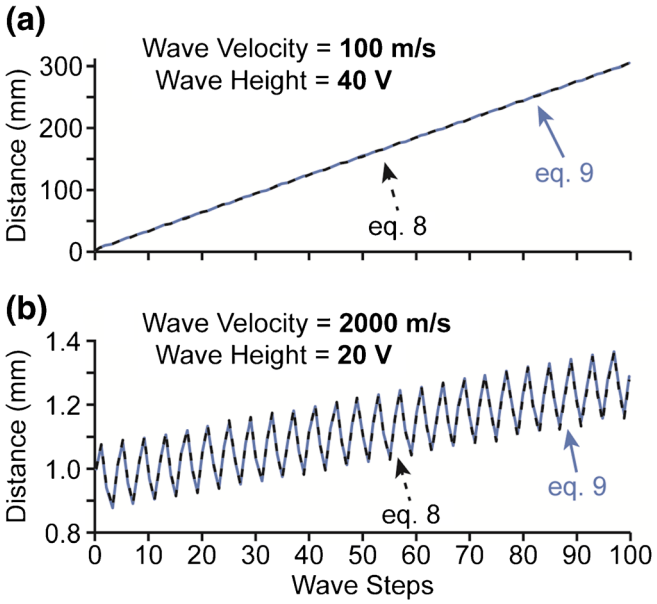

Figure 2. The total distance traveled by an ion with a 17.0 nm^2 $Da^{1/2}$ adjusted cross-section as a function of the number of waves that have passed through the TWIMS device. These results are obtained using Equation 8 (black dashed lines) and numerical integration of Equation 9 (blue lines) and instrumental settings that result in the ion **(a)** traversing the TWIMS cell at the wave velocity and **(b)** being overtaken by the traveling waves

wave once every four wave steps but on average moves forward through the device towards the detector, consistent with the motion of a low mobility ion moving through the device. Other models of the motion of ions in TWIMS devices have also shown ions traversing the TWIMS cell at the wave velocity with low wave velocities and the same ions experiencing numerous rollover events with high wave velocities [43].

The average ion drift velocity during a wave step (v_{ave}) is obtained by dividing the average distance the ion travels per wave step (d_{ave}) by the dwell time:

$$v_{ave} = \frac{d_{ave}}{t_{dwell}} \tag{10}$$

The distance the ion travels varies between wave steps, especially when the ion is overtaken by a wave. Therefore, the effect that the number of steps used has on the average distance the ion travels per wave step and, thus, on v_{ave} is investigated using conditions that result in the ion being overtaken by the traveling waves (17.0 nm^2 $Da^{1/2}$ adjusted cross-section, 20 V wave height, 2000 m/s wave velocity, Figure 3a). Under these conditions, the average ion drift velocity varies significantly for the first several steps (from 51 m/s after step 1 to –27 m/s after step 3), but the variation in the average velocity damps out quickly. With ~3650 or more steps, the variability in the average drift velocity is less than 1%, indicating that the uncertainty in the average drift velocity is negligible after ~3650 wave steps. For ions with smaller adjusted cross-sections, the waves pass by the ion less frequently, which reduces the uncertainty in the average ion drift velocity.

The drift time of an ion through the entire TWIMS device (t_{drift}) is determined from the average ion drift velocity per wave step using Equation 11:

$$t_{drift} = \frac{L_{TWIMS}}{v_{ave}} \tag{11}$$

where L_{TWIMS} is the length of the TWIMS device (254 mm). Drift times obtained with Equation 11 using values for v_{ave} obtained with Equation 8 and numerical integration of Equation 9 are shown in Figure 3b as blue circles and red diamonds, respectively. These drift times are obtained using 10,000 wave steps, a 17.0 nm^2 $Da^{1/2}$ adjusted cross-section, a 20 V wave height, and wave velocities of between 100 and 2000 m/s. The variability in the average distance traveled per wave step is less than 0.4% with 10,000 or more wave steps. Surprisingly, the drift times obtained with Equations 8 and 9 are the same to within <1.5% at each wave velocity despite the ≤11.4% difference between the electric field strengths obtained with the equations used to derive Equations 8 and 9 (Equations 3 and 4, respectively). Similar drift times may be obtained with Equations 8 and 9 because the average difference between the electric field strengths obtained with Equations 3 and 4 over a full wavelength (between $x = -6.05$ and +6.05 mm) is approximately zero (Figure 1c). Therefore, any errors that may occur in calculating the distance an ion travels in the individual steps is greatly reduced by averaging over multiple steps. Calculating

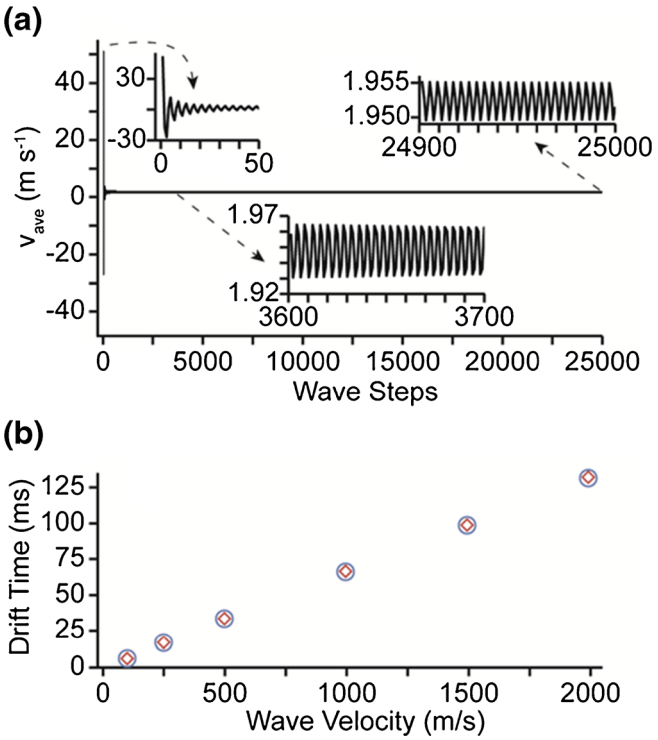

Figure 3. **(a)** The average ion drift velocity as a function of the number of wave steps that have passed through the TWIMS device obtained with a 17.0 nm^2 Da$^{1/2}$ adjusted cross-section, a 20 V wave height, and a 2000 m/s wave velocity. **(b)** Calculated drift times obtained using average ion drift velocities obtained with Equation 8 (blue circles) and numerical integration of Equation 9 (red diamonds) with a 17.0 nm^2 Da$^{1/2}$ adjusted cross-section, a 20 V wave height, and wave velocities of between 100 and 2000 m/s

a single drift time using Equation 8 takes less than 1 s, whereas the same calculation using numerical integration of Equation 9 can take more than 1 min, depending on instrument conditions. Therefore, it may be advantageous to use Equation 8 when simulating a large number of ions.

Results and Discussion

Accuracy of the Computed Drift Times

The drift times of 70 different reference ions are calculated with Equation 11 for wave velocities of between 100 and 2000 m/s and wave heights of 20 and 40 V. These wave heights and the 3.2 mbar pressure of the background gas result in maximum field strength to pressure ratios of ~15 and ~30 V cm^{-1} mbar^{-1} for the 20 and 40 V wave heights, respectively. The low-field limit is typically between ~15 and ~34 V cm^{-1} mbar^{-1} for most ions [50, 51]. Thus, the low field limit should apply when the lower wave height is used, but conditions that exceed the low field limit will exist for a fraction of the time when the higher wave height is used. In the low field limit, the ion mobility does not depend significantly on the electric field strength, but in the high field limit, the mobility of the ions may depend on the electric field strength. These calculated drift times are obtained using average distances traveled per wave step obtained with Equation 8 using 10,000 wave steps and adjusted cross-sections calculated using DTIMS cross-sectional values. The reference ions range in mass from 231 Da to 103 kDa, in charge from 1+ to 24+, and in collisional cross-section measured with DTIMS from 1.51 to 60.9 nm^2. These values correspond to adjusted cross-sections between 7.5 and 17.0 nm^2 Da$^{1/2}$. The data obtained with 20 and 40 V wave heights are shown as a function of the adjusted cross-sections calculated using DTIMS cross-sectional values in Figure 4a and b, respectively. Also shown in these respective figures are the drift times measured for the reference ions using 20 and 40 V wave heights and various wave velocities. Open and filled shapes correspond to ions formed from denaturing and buffered aqueous solutions, respectively. The unadjusted drift times obtained for the reference ions using the various wave heights and wave velocities are listed in the Supplementary Material (Tables S-1 through S-6).

The difference between the drift times that are measured in TWIMS and the calculated drift times modeled using the same experimental parameters used in the TWIMS measurements and the DTIMS cross-sectional values is small for ions formed from denaturing solutions (average difference = 2%) for wave velocities of ≤1500 m/s and both wave heights. These results indicate that TWIMS drift times for a wide variety of protein and peptide ions formed from denaturing solutions can be accurately predicted using the computational method presented here for low wave velocities. In contrast, the measured drift times acquired with a 2000 m/s wave velocity are significantly larger than the calculated drift times at this same wave velocity (average difference = 12% and 20% larger in Figure 4a and b, respectively). The difference between the measured and calculated drift times for ions generated from buffered aqueous solutions is also low for low wave velocities (average difference = 1% for wave velocities of ≤500 m/s), but the measured drift times are on average 16% and 25% larger than the calculated drift times for wave velocities of 1000 and 1500 m/s, respectively. The width of the ion mobility peaks increases as the wave velocity increases, and with the 2000 m/s wave velocity, the width of the peaks corresponding to the ions formed from buffered aqueous solutions are too broad to obtain measured drift times.

Obtaining Collisional Cross-Sections with the Computational Method

In order to obtain absolute collisional cross-sections from TWIMS drift times without experimental calibration, the computed drift times as a function of the adjusted cross-sections are fit with second-order polynomials ($R^2 = 1.00$). Although DTIMS cross-sectional values were used to calculate the computed drift times used to obtain these polynomial fits, nearly identical fits are obtained using purely hypothetical adjusted cross-sections (Supplementary Material, Figure S-1), and the relationship between adjusted cross-section and TWIMS drift

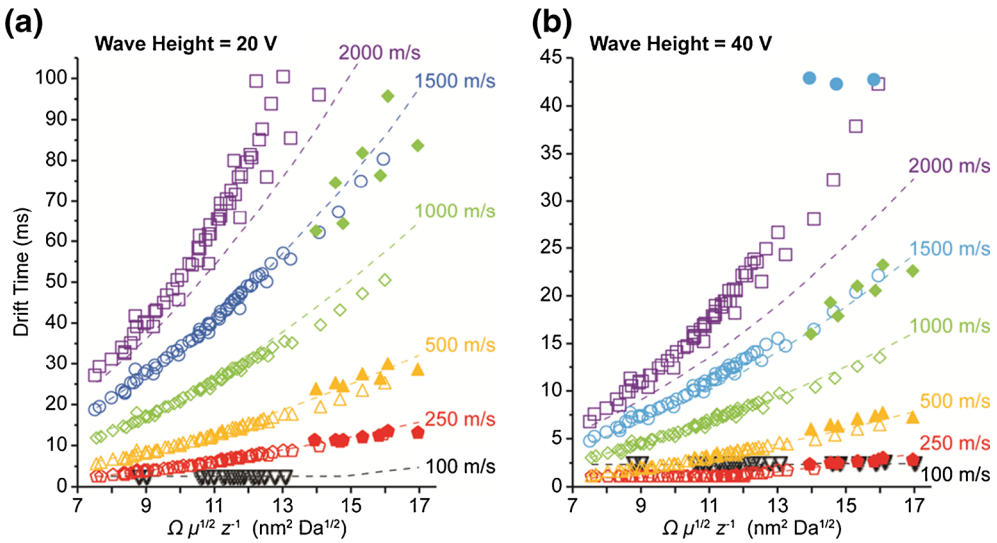

Figure 4. Measured (shapes) and calculated (dashed lines) drift times as a function of the adjusted cross-sections determined using DTIMS cross-sectional values. These results are obtained with **(a)** 20 and **(b)** 40 V wave heights and 100 (black inverted triangles), 250 (red pentagons), 500 (yellow triangles), 1000 (green diamonds), 1500 (blue circles), and 2000 (purple squares) m/s wave velocities. Open and filled shapes correspond to ions formed from denaturing and buffered aqueous solutions, respectively

time described by these polynomial fits is independent of any DTIMS cross-sectional values. Second-order polynomials are used to obtain these fits because second-order polynomials have been reported to result in the lowest absolute errors for TWIMS chemical calibration curves, compared with that obtained with linear, third-order polynomial, and natural-log fits [39]. Cross-sections were obtained from these polynomial fits and the measured drift times of the reference ions. Cross-sections are not determined for ions that traverse the TWIMS cell at the wave velocity because there is no separation for these ions and therefore only an upper limit to the mobility of the ions is obtained. The cross-sections obtained for the reference ions using the computational method with 20 and 40 V wave heights and the various wave velocities are shown as a function of the DTIMS cross-sections in Figure 5a and b, respectively, and are also listed in the Supplementary Material (Tables S-7 through S-12).

The TWIMS computational calibration cross-sections obtained for the ions formed from denaturing solutions are extremely similar to those obtained with DTIMS (average difference = 0.1%) for wave velocities of ≤1500 m/s. This uncertainty is similar to the uncertainty resulting from the standard experimental calibration approach [39] for obtaining collisional cross-sections with TWIMS (1% [34, 37–39]). These results indicate that the cross-sections for ions formed from denaturing solutions obtained using TWIMS computational calibration with low wave velocities are approximately as accurate as those obtained using TWIMS chemical calibration.

Significantly larger cross-sections are obtained for the ions formed from denaturing solutions with TWIMS computational calibration with a 2000 m/s wave velocity than are obtained with DTIMS at both 20 and 40 V wave heights (on average 7% and 12% larger in Figure 5a and b, respectively). The difference in the cross-sections obtained here using a 2000 m/s wave velocity and those obtained with DTIMS generally increases with ion drift time for a given wave height (Figure 6a and b, respectively). Surprisingly, this deviation is much less for singly protonated polyalanine compared with the multiply protonated ion data. The drift times at a 20 V wave height are about four times longer than those at 40 V. However, the magnitude of the deviation with the DTIMS values is higher with the 40 V wave height. Thus, the deviation with DTIMS values for a given time that the ions spend in the TWIMS device is less when the lower wave height is used. This may be because the lower wave height results in conditions that are in the low field limit at all times, whereas ions can spend some fraction of time outside of this limit with the 40 V wave height. It may also be due to factors not included in this model. These results indicate that the errors in the cross-sectional values obtained with the 2000 m/s wave velocity do not result directly from either the number of rollover events experienced by the ions or the length of time the ions spend in the TWIMS device, but rather on wave height and possibly some other factors. This effect is most apparent only at the highest wave velocity. High-order effects that depend on wave velocity could include the time required to achieve force-balance, the confining rf, or the rise time of the power supply used to generate the potential wave. It is unclear why these factors would result in the lower deviation observed for singly protonated polyalanine compared with the multiply charged ions, suggesting that conformational changes, which are less accessible to a singly charged ion, may also play a role.

The collisional cross-sections obtained here with low wave velocities (≤500 m/s) for ions formed from buffered aqueous solutions are also very similar to those obtained with DTIMS (average difference = 1%, Figure 5, upper panels), but with

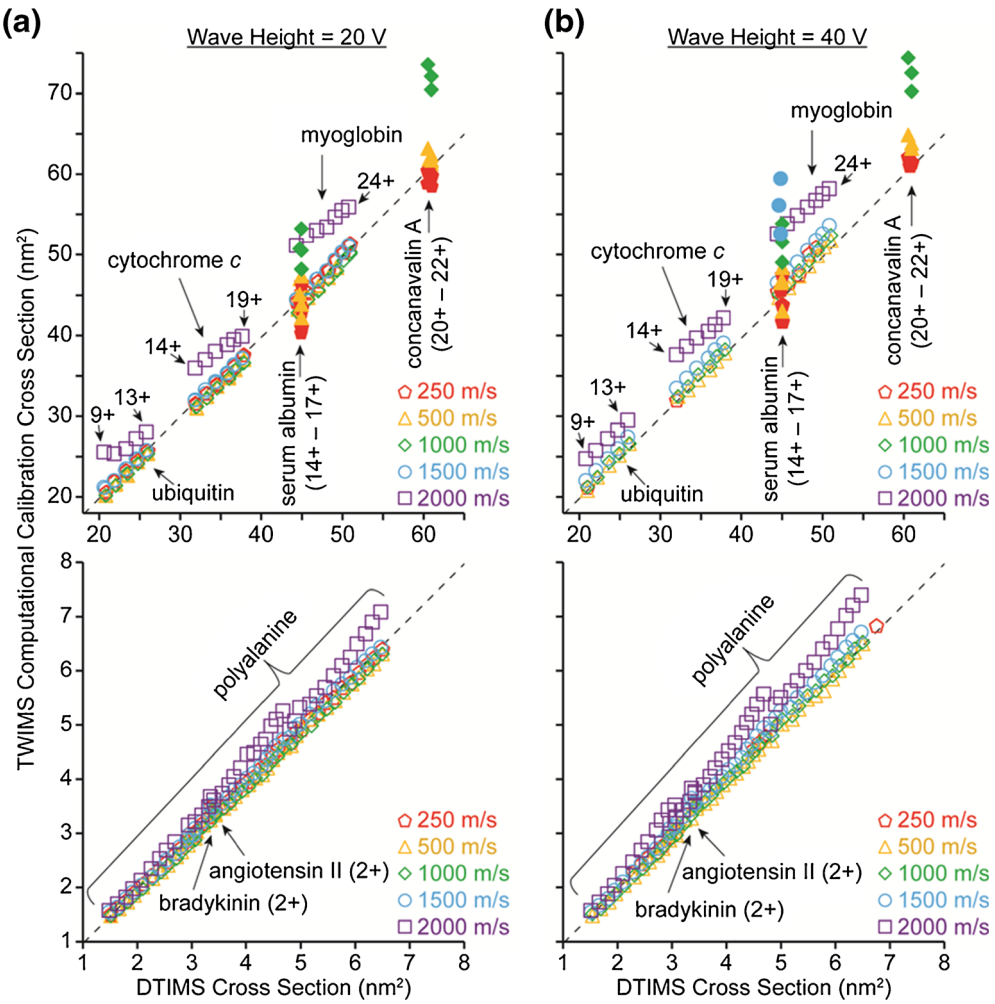

Figure 5. TWIMS computational calibration cross-sections obtained with **(a)** 20 and **(b)** 40 V wave heights and 250 (red pentagons), 500 (yellow triangles), 1000 (green diamonds), 1500 (blue circles), and 2000 (purple squares) *m/s* wave velocities as a function of the corresponding DTIMS cross-sections. Open and closed shapes correspond to ions formed from denaturing and buffered aqueous solutions, respectively. Black dashed lines are a one-to-one correspondence between the axes

1000 and 1500 m/s wave velocities, the cross-sections obtained here are on average 16% and 25% larger, respectively, than those obtained with DTIMS. In striking contrast, the average difference is only 1% for the ions formed from denaturing solutions at these two higher wave velocities. The higher cross-sections obtained for the ions formed from the buffered aqueous solutions in which folded structures are adopted are consistent with these ions unfolding during TWIMS [41, 48].

The difference in the relationship between wave velocity and drift time for folded and unfolded protein ions has been reported previously [38, 41, 47, 48]. This effect has been attributed to conformation effects [41] and other unspecified factors, which result in longer drift times for folded protein ions than for unfolded protein ions [38]. Ion heating inside TWIMS devices has been investigated previously by measuring the extent to which ions with known Arrhenius parameters (benzylpyridinium ions, protonated leucine enkephalin dimer, and *holo*-myoglobin) dissociate during TWIMS separation [46–48]. In a second generation TWIMS device, such as that used here, dissociation from ion heating was observed upon injection of ions into the TWIMS device, and the effective temperature of the ions decreased with increasing wave velocity [47, 48]. In addition, the ratio of folded to unfolded ubiquitin 6+ conformers depends on some parameters [47, 54] but not on the wave height or wave velocity [54]. Thus, excess ion heating should not occur at the higher wave velocities used here during TWIMS. It is possible that ion heating upon injection may result in destabilization and subsequent unfolding of the ions during TWIMS with more unfolding occurring at the higher wave velocities owing to the longer drift times and thus more time for unfolding to occur. It is also possible that other high order factors, such as the time required to achieve force-balance, the rise time of the power supply, or effects from the confining rf also play a role. Higher *m/z* ions, such as those formed from buffered aqueous solutions, may experience more of these higher order factors, such as a greater extent of the population slightly off the central axis and thus exposed to different electric fields. Interestingly, data for Cs^+ indicate that the cross-section varies by less than 1.0% with the same range of wave heights and wave velocities used for the

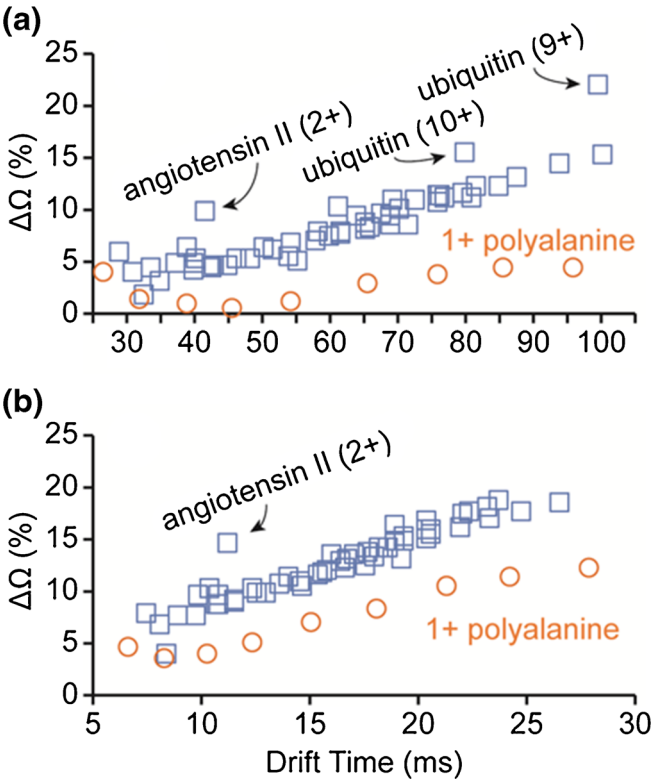

Figure 6. Difference between the collisional cross-sections of ions formed from denaturing solutions obtained with the computational method with **(a)** 20 and **(b)** 40 V wave heights and a 2000 m/s wave velocity and those obtained with DTIMS as a function of drift time. Circles correspond to 1+ polyalanine ions and squares correspond to all other ions

protein data. Cs^+ cannot undergo a conformational change and appears to be unaffected by these other high order factors. It is also unclear how these other factors would result in longer transit times for folded protein ions than for unfolded protein ions with similar adjusted cross-sections. Thus, conformational changes may play a role in the protein data.

In summary, the results in Figure 5 indicate that computational calibration of TWIMS can be used to obtain absolute collisional cross-sections of protein and peptide ions formed from both denaturing and buffered aqueous solutions that are similar to those obtained with DTIMS, but that low wave velocities and gentle instrument settings should be used to minimize any uncertainties resulting from high-order effects not accounted for in the present model and from any unfolding that might occur.

Conclusions

A method for calibrating TWIMS drift times using computational simulations in order to obtain collisional cross-sections is presented. The accuracy of this method is assessed by comparing the collisional cross-sections of 70 different reference ions obtained using this method with those reported from DTIMS measurements. The cross-sections obtained here with low wave velocities are very similar to those obtained with DTIMS (average difference = 0.3%), both for ions formed from denaturing solutions and for those formed from buffered aqueous solutions. These results demonstrate that collisional cross-sections can be obtained from a single TWIMS drift time measurement without prior experimental calibration. The method presented here does not include a discrete description of the collision events that occur between the ions and the buffer gas nor does it account for the identity of the buffer gas. This significant limitation of the model could be improved by including a term describing the intermolecular potentials between the ions and the buffer gas. This improvement would make it possible to extend this method for use with a variety of buffer gases. This method also does not include corrections for surface topology [55] or pressure gradients along the axis of the device. Moreover, a rough approximation that force-balance is achieved instantaneously is made in the derivation of this model. Despite these significant deficiencies, the uncertainty in the collisional cross-sections obtained using this method is about the same as that obtained using the more conventional TWIMS experimental calibration approach. Therefore, this technique can eliminate the need for experimental calibration, although further experiments are needed to determine the effects of other variables, such as pressure, bias voltage, and scan frequency, on the accuracy of this method.

The collisional cross-sections of protein and peptide ions obtained here with high wave velocities are larger than those obtained with DTIMS, especially for those formed from buffered aqueous solutions. These higher than expected cross-sections could be the result of high-order effects not accounted for in the present model. Data obtained with high wave velocities (≥1000 m/s) for the ions formed from buffered aqueous solutions may also be consistent with the protein ions unfolding during TWIMS. These results indicate that low wave velocities should be used for obtaining collisional cross-sections with TWIMS in order to minimize any uncertainties that may result from high-order effects or from changes in protein ion conformation that can occur during TWIMS. The resolution of TWIMS measurements increases with increasing wave velocity [44]. Therefore, a balance must be struck between resolution and accuracy when selecting the TWIMS wave velocity. The accuracy of the TWIMS computational calibration cross-sections also depends on the accuracy to which the pressure inside the TWIMS cell is known. It should be possible to calibrate the pressure in a TWIMS drift cell by measuring the drift time of an ion that will not likely undergo a conformational change during TWIMS, such as C_{60} [30] or bovine pancreatic trypsin inhibitor [10]. The pressure used to calculate the drift time of such an ion can be varied until a value similar to the measured drift time is obtained. With a calibrated pressure, adjusted collisional cross-sections can be obtained with TWIMS by computing drift times using purely hypothetical adjusted cross-sections in order to obtain a second-order polynomial function that relates drift times to adjusted cross-sections. The range of adjusted cross-sections in these calculations should be chosen so as to bracket the measured drift times to be

calibrated. The absolute cross-section can be obtained from the adjusted cross-section with the reduced mass and ion charge. The latter can be readily obtained when isotopic resolution is achieved or from the *m*/*z* spacing between molecular ions in less complex samples.

Acknowledgements

The authors thank the reviewers of this manuscript for thoughtful comments and suggestions, the UCSF Sandler-Moore Mass Spectrometry Core Facility for use of their Synapt G2 instrument, and the National Institutes of Health for funding (R01GM097357 and S10OD020062). The authors are also thankful for the pioneering contributions made by Professor Scott A. McLuckey in the fields of mass spectrometry instrumentation and methods development and gas-phase ion chemistry.

References

1. Mason, E.A., McDaniel, E.W. (eds.): Transport properties of ions in gases. Wiley, New York (1988)
2. Cohen, M.J., Karasek, F.W.: Plasma chromatography - a new dimension for gas chromatography and mass spectrometry. J. Chromatogr. Sci. **8**, 330–337 (1970)
3. Bowers, M.T., Kemper, P.R., Vonhelden, G., Vankoppen, P.A.M.: Gas-phase ion chromatography - transition-metal state selection and carbon cluster formation. Science **260**, 1446–1451 (1993)
4. St. Louis, R.H., Hill, H.H.J., Eiceman, G.A.: Ion mobility spectrometry in analytical chemistry. Crit. Rev. Anal. Chem. **21**, 321–356 (1990)
5. Jarrold, M.F.: Drift-tube studies of atomic clusters. J. Phys. Chem. **99**, 11–21 (1995)
6. Valentine, S.J., Counterman, A.E., Hoaglund-Hyzer, C.S., Clemmer, D.E.: Intrinsic amino acid size parameters from a series of 113 lysine-terminated tryptic digest peptide ions. J. Phys. Chem. B **103**, 1203–1207 (1999)
7. Kaur-Atwal, G., Weston, D.J., Green, P.S., Crosland, S., Bonner, P.L.R., Creaser, C.S.: Analysis of tryptic peptides using desorption electrospray ionization combined with ion mobility spectrometry/mass spectrometry. Rapid Commun. Mass Spectrom. **21**, 1131–1138 (2007)
8. Djidja, M.C., Francese, S., Loadman, P.M., Sutton, C.W., Scriven, P., Claude, E., Snel, M.F., Franck, J., Salzet, M., Clench, M.R.: Detergent addition to tryptic digests and ion mobility separation prior to MS/MS improves peptide yield and protein identification for in situ proteomic investigation of frozen and formalin-fixed paraffin-embedded adenocarcinoma tissue sections. Proteomics **9**, 2750–2763 (2009)
9. Stauber, J., MacAleese, L., Franck, J., Claude, E., Snel, M., Kaletas, B.K., Wiel, I.M.V.D., Wisztorski, M., Fournier, I., Heeren, R.M.A.: On-tissue protein identification and imaging by MALDI-ion mobility mass spectrometry. J. Am. Soc. Mass Spectrom. **21**, 338–347 (2010)
10. Shelimov, K.B., Clemmer, D.E., Hudgins, R.R., Jarrold, M.F.: Protein structure *in vacuo*: gas-phase conformations of BPTI and cytochrome *c*. J. Am. Chem. Soc. **119**, 2240–2248 (1997)
11. Badman, E.R., Hoaglund-Hyzer, C.S., Clemmer, D.E.: Monitoring structural changes of proteins in an ion trap over similar to 10-200 Ms: unfolding transitions in cytochrome *c* ions. Anal. Chem. **73**, 6000–6007 (2001)
12. Thalassinos, K., Slade, S.E., Jennings, K.R., Scrivens, J.H., Giles, K., Wildgoose, J., Hoyes, J., Bateman, R.H., Bowers, M.T.: Ion mobility mass spectrometry of proteins in a modified commercial mass spectrometer. Int. J. Mass Spectrom. **236**, 55–63 (2004)
13. Shi, L., Holliday, A.E., Glover, M.S., Ewing, M.A., Russell, D.H., Clemmer, D.E.: Ion mobility-mass spectrometry reveals the energetics of intermediates that guide polyproline folding. J. Am. Soc. Mass Spectrom. **27**, 22–30 (2016)
14. Ruotolo, B.T., Giles, K., Campuzano, I., Sandercock, A.M., Bateman, R.H., Robinson, C.V.: Evidence for macromolecular protein rings in the absence of bulk water. Science **310**, 1658–1661 (2005)
15. Loo, J.A., Berhane, B., Kaddis, C.S., Wooding, K.M., Xie, Y.M., Kaufman, S.L., Chernushevich, I.V.: Electrospray ionization mass spectrometry and ion mobility analysis of the 20s proteasome complex. J. Am. Soc. Mass Spectrom. **16**, 998–1008 (2005)
16. Uetrecht, C., Versluis, C., Watts, N.R., Wingfield, P.T., Steven, A.C., Heck, A.J.R.: Stability and shape of hepatitis B virus capsids in vacuo. Angew. Chem. Int. Ed. **47**, 6247–6251 (2008)
17. Thomas, J.J., Bothner, B., Traina, J., Benner, W.H., Siuzdak, G.: Electrospray ion mobility spectrometry of intact viruses. Spectrosc. Int. J. **18**, 31–36 (2004)
18. McDaniel, E.W., Barnes, W.S., Martin, D.W.: Drift tube-mass spectrometer for studies of low-energy ion-molecule reactions. Rev. Sci. Instrum. **33**, 2–6 (1962)
19. Hoaglund, C.S., Valentine, S.J., Sporleder, C.R., Reilly, J.P., Clemmer, D.E.: Three-dimensional ion mobility/TOFMS analysis of electrosprayed biomolecules. Anal. Chem. **70**, 2236–2242 (1998)
20. Tang, K.Q., Li, F.M., Shvartsburg, A.A., Strittmatter, E.F., Smith, R.D.: Two-dimensional gas-phase separations coupled to mass spectrometry for analysis of complex mixtures. Anal. Chem. **77**, 6381–6388 (2005)
21. Purves, R.W., Guevremont, R.: Electrospray ionization high-field asymmetric waveform ion mobility spectrometry-mass spectrometry. Anal. Chem. **71**, 2346–2357 (1999)
22. Robinson, E.W., Williams, E.R.: Multidimensional separations of ubiquitin conformers in the gas phase: relating ion cross-sections to H/D exchange measurements. J. Am. Soc. Mass Spectrom. **16**, 1427–1437 (2005)
23. Shvartsburg, A.A., Li, F.M., Tang, K.Q., Smith, R.D.: High-resolution field asymmetric waveform ion mobility spectrometry using new planar geometry analyzers. Anal. Chem. **78**, 3706–3714 (2006)
24. Räsänen, R., Nousiainen, M., Peräkorpi, K., Sillanpää, M., Polari, L., Anttalainen, O., Utriainen, M.: Determination of gas phase triacetone triperoxide with aspiration ion mobility spectrometry and gas chromatography-mass spectrometry. Anal. Chim. Acta **623**, 59–65 (2008)
25. Arnanthigo, Y., Anttalainen, O., Safaei, Z., Sillanpää, M.: Sniff-testing for indoor air contaminants from new buildings environment detecting by aspiration-type ion mobility spectrometry. Int. J. Ion Mobil. Spectrom. **19**, 15–30 (2016)
26. Giles, K., Williams, J.P., Pringle, S.D., Wildgoose, J.L., Slade, S.E., Thalassinos, K., Bateman, R.H., Bowers, M.T., Scrivens, J.H.: An investigation of the mobility separation of some peptide and protein ions using a new hybrid quadrupole/traveling wave IMS/Oa-ToF Instrument. Int. J. Mass Spectrom. **261**, 1–12 (2007)
27. Giles, K., Williams, J.P., Campuzano, I.: Enhancements in traveling wave ion mobility resolution. Rapid Commun. Mass Spectrom. **25**, 1559–1566 (2011)
28. Giles, K., Pringle, S.D., Worthington, K.R., Little, D., Wildgoose, J.L., Bateman, R.H.: Applications of a traveling wave-based radio-frequency-only stacked ring ion guide. Rapid Commun. Mass Spectrom. **18**, 2401–2414 (2004)
29. Shvartsburg, A.A., Smith, R.D.: Fundamentals of traveling wave ion mobility spectrometry. Anal. Chem. **80**, 9689–9699 (2008)
30. Wyttenbach, T., von Helden, G., Batka Jr., J.J., Carlat, D., Bowers, M.T.: Effect of the long-range potential on ion mobility measurements. J. Am. Soc. Mass Spectrom. **8**, 275–282 (1997)
31. Kanu, A.B., Dwivedi, P., Tam, M., Matz, L., Hill Jr., H.H.: Ion mobility-mass spectrometry. J. Mass Spectrom. **43**, 1–22 (2008)
32. Bohrer, B.C., Merenbloom, S.I., Koeniger, S.L., Hilderbrand, A.E., Clemmer, D.E.: Biomolecule analysis by ion mobility spectrometry. Annu. Rev. Anal. Chem. **1**, 293–327 (2008)
33. Ruotolo, B.T., Benesch, J.L.P., Sandercock, A.M., Hyung, S., Robinson, C.V.: Ion mobility-mass spectrometry analysis of large protein complexes. Nat. Protoc. **3**, 1139–1152 (2008)
34. Thalassinos, K., Grabenauer, M., Slade, S.E., Hilton, G.R., Bowers, M.T., Scrivens, J.H.: Characterization of phosphorylated peptides using traveling wave-based and drift cell ion mobility mass spectrometry. Anal. Chem. **81**, 248–254 (2009)
35. Smith, D.P., Knapman, T.W., Campuzano, I., Malham, R.W., Berryman, J.T., Radford, S.E., Ashcroft, A.E.: Deciphering drift time measurements from traveling wave ion mobility spectrometry-mass spectrometry studies. Eur. J. Mass Spectrom. **15**, 113–130 (2009)

36. Lanucara, F., Holman, S.W., Gray, C.J., Eyers, C.E.: The power of ion mobility-mass spectrometry for structural characterization and the study of conformational dynamics. Nat. Chem. **6**, 281–294 (2014)
37. Ridenour, W.B., Kliman, M., McLean, J.A., Caprioli, R.M.: Structural characterization of phospholipids and peptides directly from tissue sections by MALDI traveling-wave ion mobility-mass spectrometry. Anal. Chem. **82**, 1881–1889 (2010)
38. Salbo, R., Bush, M.F., Naver, H., Campuzano, I., Robinson, C.V., Pettersson, I., Jorgensen, T.J.D., Haselmann, K.F.: Traveling-wave ion mobility mass spectrometry of protein complexes: accurate calibrated collision cross-sections of human insulin oligomers. Rapid Commun. Mass Spectrom. **26**, 1181–1193 (2012)
39. Bush, M.F., Campuzano, I.D.G., Robinson, C.V.: Ion mobility mass spectrometry of peptide ions: effects of drift gas and calibration strategies. Anal. Chem. **84**, 7124–7130 (2012)
40. Bush, M.F., Hall, Z., Giles, K., Hoyes, J., Robinson, C.V., Ruotolo, B.T.: Collision cross-sections of proteins and their complexes: a calibration framework and database for gas-phase structural biology. Anal. Chem. **82**, 9557–9565 (2010)
41. Michaelevski, I., Eisenstein, M., Sharon, M.: Gas-phase compaction and unfolding of protein structures. Anal. Chem. **82**, 9484–9491 (2010)
42. Giles, K., Wildgoose, J.L., Langridge, D.J., Campuzano, I.: A method for direct measurement of ion mobilities using a traveling wave ion guide. Int. J. Mass Spectrom. **298**, 10–16 (2010)
43. May, J.C., McLean, J.A.: The influence of drift gas composition on the separation mechanism in traveling wave ion mobility spectrometry: insight from electrodynamic simulations. Int. J. Ion Mobil. Spectrom. **16**, 85–94 (2013)
44. Hamid, A.M., Ibrahim, Y.M., Garimella, S.V.B., Webb, I.K., Deng, L., Chen, T., Anderson, G.A., Prost, S.A., Norheim, R.V., Tolmachev, A.V., Smith, R.D.: Characterization of traveling wave ion mobility separations in structures for lossless ion manipulations. Anal. Chem. **87**, 11301–11308 (2015)
45. Ruotolo, B.T., Hyung, S., Robinson, P.M., Giles, K., Bateman, R.H., Robinson, C.V.: Ion mobility-mass spectrometry reveals long-lived, unfolded intermediates in the dissociation of protein complexes. Angew. Chem. Int. Ed. **46**, 8001–8004 (2007)
46. Morsa, D., Gabelica, V., De Pauw, E.: Effective temperature of ions in traveling wave ion mobility spectrometry. Anal. Chem. **83**, 5775–5782 (2011)
47. Merenbloom, S.I., Flick, T.G., Williams, E.R.: How hot are your ions in TWAVE ion mobility spectrometry? J. Am. Soc. Mass Spectrom. **23**, 553–562 (2012)
48. Morsa, D., Gabelica, V., De Pauw, E.: Fragmentation and isomerization due to field heating in traveling wave ion mobility spectrometry. J. Am. Soc. Mass Spectrom. **25**, 1384–1393 (2014)
49. Manura, D., Dahl, D.A.: SIMION version 8.04. Scientific Instrument Services, Inc., Ringoes (2006)
50. Valentine, S., Counterman, A., Clemmer, D.: A database of 660 peptide ion cross-sections: use of intrinsic size parameters for bona fide predictions of cross-sections. J. Am. Soc. Mass Spectrom. **10**, 1188–1211 (1999)
51. Verbeck, G., Ruotolo, B., Gillig, K., Russell, D.: Resolution equations for high-field ion mobility. J. Am. Soc. Mass Spectrom. **15**, 1320–1324 (2004)
52. Johnsen, R., Biondi, M.A.: Reaction-rates of uranium ions and atoms with O_2 and N_2. J. Chem. Phys. **57**, 1975–1979 (1972)
53. Bleiholder, C.: Towards measuring ion mobilities in non-stationary gases and non-uniform and dynamic electric fields (I). Transport equation. Int. J. Mass Spectrom. **399**, 1–9 (2016)
54. Chen, S., Russell, D.H.: How closely related are conformations of protein ions sampled by IM-MS to native solution structures? J. Am. Soc. Mass Spectrom. **26**, 1433–1443 (2015)
55. Wyttenbach, T., Bleiholder, C., Anderson, S.E., Bowers, M.T.: A new algorithm to characterize the degree of concaveness of a molecular surface relevant in ion mobility spectrometry. Mol. Phys. **113**, 2344–2349 (2015)